Imaging Neuroscience
an open access journal

Research Article

Detecting glioblastoma infiltration beyond conventional imaging tumour margins using MTE-NODDI

Saketh R. Karamched[a,b,*], Dunja Gorup[a,*], Daniele Tolomeo[c], Lucy J. Brooks[b], Ting Gong[d], Andreas Christ Sølvsten Jørgensen[e,f], Ciaran Scott Hill[b,g], Melanie Clements[b], Tammy L. Kalber[a], Jack A. Wells[a], Daniel J. Stuckey[a], Lewis Thorne[g], Vahid Shahrezaei[e], Samuel Marguerat[h], Hui Zhang[d], Simona Parrinello[b], Mark F. Lythgoe[a]

[a]UCL Centre for Advanced Biomedical Imaging, Division of Medicine, University College London, London, United Kingdom
[b]Samantha Dickson Brain Cancer Unit, UCL Cancer Institute, London, United Kingdom
[c]IXICO plc, London, United Kingdom
[d]UCL Hawkes Institute, Department of Computer Science, University College London, London, United Kingdom
[e]Department of Mathematics, Faculty of Natural Sciences, Imperial College London, London, United Kingdom
[f]I-X Centre for AI In Science, Imperial College London, London, United Kingdom
[g]Department of Neurosurgery, The National Hospital for Neurology and Neurosurgery, London, United Kingdom
[h]UCL Cancer Institute, London, United Kingdom

*Joint first author

Corresponding Author: Mark F. Lythgoe (m.lythgoe@ucl.ac.uk)

ABSTRACT

Glioblastoma (GBM) is the most common and aggressive brain tumour with stark resistance to available therapies, leading to relapse and a median survival of <15 months. A key cause of therapy resistance is diffuse infiltration of tumour cells into brain regions surrounding the tumour, which presents a major clinical challenge as existing imaging techniques offer limited detection of the resectable margin. Here, we use diffusion weighted imaging (DWI) and apply the multiple echo time neurite orientation dispersion and density imaging (MTE-NODDI) model as a tool to detect tumour cells in the hard-to-distinguish margin. We used the G144 patient-derived xenograft model, with characteristic invasion along white matter tracts, in combination with MTE-NODDI. Tumour development was monitored, and magnetic resonance imaging (MRI) data were acquired over a 4-week period, starting at 4 weeks after stereotactic injection of tumour cells. MTE-NODDI demonstrated sensitivity to the developing tumour in the invading margin, and changes in measured parameters were apparent from 6 weeks after injection. In comparison to standard DWI, MTE-NODDI showed increased sensitivity to the tumour-associated changes in the margin. Furthermore, extraneurite volume fraction (f_{en}) and neurite density index (NDI) measured from MTE-NODDI correlated with immunohistological measurement of tumour cells. These findings suggest that MTE-NODDI may non-invasively detect infiltrating cells and tumour-induced pathology in margin regions without T2 or DWI changes in a patient-derived mouse model of GBM. MTE-NODDI is clinically translatable and could be a powerful tool for neurosurgeons to maximise surgical resection, resulting in better survival outcomes for patients with GBM.

Keywords: glioblastoma, tumour cells, tumour invasion, diffusion-weighted imaging, NODDI, multiple echo-time NODDI, imaging biomarkers, translational imaging

Received: 8 January 2024 Revision: 10 September 2024 Accepted: 6 January 2025 Available Online: 30 January 2025

1. INTRODUCTION

Glioblastoma (GBM) is the most common and aggressive primary brain tumour in adults (Omuro & DeAngelis, 2013). The current standard of care includes maximal safe surgical resection followed by radiotherapy and concomitant chemotherapy with temozolomide (Stupp et al., 2005). Despite such active treatment strategies, the prognosis remains extremely poor and the outcome for nearly all patients is dismal, with a median survival of <15 months and an average 5-year survival rate of <5% (Miller et al., 2021). The key cause of resistance to available treatments is diffuse infiltration of tumour cells into the normal brain parenchyma, a hallmark of GBM (Cuddapah et al., 2014; Vehlow & Cordes, 2013). Infiltration precludes curative surgery and causes recurrence from low numbers of cells that have invaded past the margin of original resection. Radiotherapy target volumes are planned to account for an unseen population of invading tumour cells into healthy tissues that can extend beyond the gross tumour volume (Niyazi et al., 2023), yet tumour recurrence occurs, possibly indicating migrating tumour cells outside the planned treatment area. As cell invasion may not be uniform from the tumour bulk, an image-guided approach may provide a method to more closely map migrating tumour cells and thus allowing a more precisely tailored therapy plan. Invasion in GBM is thus a major clinical challenge because traditional imaging methods, which include post-gadolinium contrast-enhanced T1-weighted, T2-weighted and fluid attenuated inversion recovery (FLAIR) MRI, cannot detect these infiltrating cells, making it impossible to accurately determine tumour margins (Lasocki & Gaillard, 2019; Price & Gillard, 2011). Other methods to aid tumour delineation include 5-aminolevulinic acid (5-ALA)-guided surgery as an adjunct to maximise resection (Hadjipanayis et al., 2015; Schatlo et al., 2015; Stepp & Stummer, 2018; Stummer et al., 2006) and intraoperative MRI (Kubben et al., 2011; Schatlo et al., 2015). However, these imaging techniques offer limited identification of the invading margin, which inevitably leads to tumour recurrence within 2 cm of the original tumour site in 80–90% of cases (Chamberlain, 2011; Claes et al., 2007; De Bonis et al., 2013; Petrecca et al., 2013; Vehlow & Cordes, 2013). Recent studies utilising magnetic resonance spectroscopy (MRS) (Laack et al., 2021), ^{18}F-DOPA positron emission tomography (PET) (Laack et al., 2021), and advanced MRI (Kim et al., 2021) for dose-escalated radiation therapy have shown early promise, suggesting that improving tumour volume definition can lead to better treatment planning in GBM.

Diffusion weighted imaging (DWI) is sensitive to diffusion of water molecules in biological tissues. DWI techniques provide non-invasive indices associated with the pattern of water diffusion, which reflect tissue microstructure (Basser et al., 1994; Le Bihan, 2014). As GBM cells infiltrate away from the tumour bulk into adjacent brain tissues, they confront new and heterogenous microenvironments, resulting in tumour-affected changes to the underlying tissue. As such, DWI may provide improved sensitivity to microstructural changes caused by the invading tumour, in turn delineating margins outside the traditionally identified tumour bulk (Maier et al., 2010; Sugahara et al., 1999; Thoeny & Ross, 2010). Neurite orientation dispersion and density imaging (NODDI) is an advanced method of DWI, which uses a biophysical compartment-based model for studying microstructural changes of brain tissue (Zhang et al., 2012). NODDI assumes that the signal measured from each tissue voxel originates from a combination of three types of microstructural compartments: intra-neurite, extra-neurite, and free water volume fractions, each of which have a unique effect on water diffusion within the environment. This allows for compartment-specific markers of microstructural properties to be determined, such as the neurite density index (NDI) (the fraction of tissue that comprises neurites; axons or dendrites), the extra-neurite volume fraction (f_{en}) (the fraction of tissue other than the neurites including microglia, astrocytes, oligodendrocytes, soma, ependymal cells, extra-cellular matrices, and vasculature), and orientation dispersion index (ODI), which reflects the spatial configuration of the neurite structures (Zhang et al., 2012). NODDI-derived measures are sensitive to altered tissue microstructure in brain development, maturation, and aging (Cox et al., 2016; Kamiya et al., 2020), as well as numerous neuropathological conditions (Churchill et al., 2019; Colgan et al., 2016; Fu et al., 2020; Kamagata et al., 2017; Kamiya et al., 2020; Kraguljac et al., 2021; Mastropietro et al., 2019; Mitchell et al., 2019; Nazeri et al., 2017; Palacios et al., 2020; Parker et al., 2018; Schneider et al., 2017; Sone et al., 2018; Spano et al., 2018; Z. Wang et al., 2019; Winston et al., 2014). Previous studies have reported the application of NODDI in investigating brain tumour bulk, differentiating primary and metastatic tumours (Caverzasi et al., 2016; Kadota et al., 2020; Mao et al., 2020), as well as regions of oedema within tumours (Masjoodi et al., 2018; Okita et al., 2023), and tumour grading (Figini et al., 2018; Maximov et al., 2017; Wen et al., 2015; Zhao et al., 2018).

NODDI is still an emerging technology, akin to contemporary compartmental models of DWI. Currently, the existing NODDI model (Zhang et al., 2012) does not account for differences in T2 relaxation between the model compartments. Therefore, when differences in compartmental T2 exist, it is difficult to disentangle differences in diffusion from relaxation. This results in

suboptimal estimation of the NODDI parameters, with overestimation of the free-water volume fraction leading to inaccuracies in measurements of NDI and ODI (Bouyagoub et al., 2016), potentially impacting the application of NODDI to conditions with T2 changes, such as in tumour tissue (Lampinen et al., 2019; Wen et al., 2015). Gong et al. (2020) recently proposed the multiple echo time NODDI (MTE-NODDI) technique, which provides robust estimates of the non-T2-weighted NODDI parameters and compartment-specific T2 values from diffusion data acquired at multiple echo times. With its ability to provide the same NODDI measures with improved parameter precision, MTE-NODDI may enhance the conspicuity of neuropathology, including imaging of brain tumours and the invading margin.

Therefore, in this study, we investigate the effectiveness of MTE-NODDI as a non-invasive *in vivo* imaging technique to improve detection of the tumour margin and demonstrate sensitivity of the technique to infiltrating tumour cells in a well-characterised patient-derived xenograft mouse model of GBM. We further report correlations of MTE-NODDI parameters with fluorescence intensity from green fluorescent protein (GFP) positive tumour cells and evaluate the technique's specificity to tumour-induced microstructural pathology.

2. MATERIALS AND METHODS

All procedures were performed in compliance with the Animal Scientific Procedures Act, 1986 and approved by the UCL Animal Welfare and Ethical Review Body (AWERB) in accordance with the international guidelines of the Home Office (UK).

2.1. Glioblastoma mouse model

A patient-derived xenograft mouse model of GBM was used in the current study. The patient (G144) was diagnosed with malignant astrocytoma (GBM), with increased copy numbers of chromosome 7 (EGFR genes map to this chromosome) (Pollard et al., 2009). Xenografts were performed on CD-1 nude mice using the G144 cell line which shows propensity for invasion through the white matter into the contralateral hemisphere. The tumour model utilised in this study was originally established in female mice (Brooks et al., 2021; Pollard et al., 2009) and, as such, only female mice were used. 8–12 week-old immunocompromised mice (n = 7) (purchased from Charles River Laboratories) underwent stereotactic implantation of 1 x 10^5 GFP-labelled G144 cells (anteroposterior 0, mediolateral -2.5, dorsoventral -3). The tumour model used in this study shows high latency with all the mice presenting tumours and they were imaged at three timepoints post injection; 4, 6, and 8 weeks, following which they were sacrificed. A separate group of age- and strain-matched naïve mice (n=3) were used in a control experiment and underwent the same imaging protocol as above.

2.2. Animal preparation for MRI

Prior to commencing the MRI acquisitions, the mice were placed in an induction chamber and anesthetised with inhaled isoflurane (2% isoflurane at 1 l/min O_2) until withdrawal reflex was lost. They were then transferred into the MRI mouse cradle with bite bar, nose cone, and ear bars to ensure a well-secured head position to minimise motion artifacts. Eye ointment was applied to prevent drying. Temperature and breathing rate were monitored throughout all the experiments using a rectal probe and a respiration pad (SA Instruments). Core body temperature was maintained at 37 ± 0.5°C via regulation of an adjustable temperature water bath. Isoflurane level was manually adjusted throughout the duration of the scan to maintain a consistent respiration rate of ~100 bpm.

2.3. Mouse MRI protocols

Images were acquired on a 9.4 T Bruker imaging system (BioSpec 94/20 USR) with a horizontal bore and 440 mT/m gradient set with an outer/inner diameter of 205 mm/116 mm, respectively (BioSpec B-GA 12S2), 86 mm volume coil, and a four-channel array receiver-surface coil (RAPID Biomedical GmbH) for the transmission and reception of RF signal. Tumours were localised using a structural T2-TurboRARE sequence (fast-spin echo, Paravision v6.0.1). The olfactory bulbs were used as an anatomical landmark to maintain consistency in slice positioning between subjects, and the slices covered the cortex and all subcortical structures up to the cerebellum. Imaging parameters for the T2-weighted acquisition were as follows: TR = 4000 ms, TE = 45 ms, FOV = 21 x 16 mm^2, data matrix 256 x 196, and 14 x 600 µm coronal slices.

For MTE-NODDI, DWI images were acquired using a 4-shot spin echo-planar imaging (EPI) sequence. Imaging parameters were: 14 slices, slice thickness = 600 µm; FOV = 20 x 16 mm^2; data matrix 110 x 85; and TR= 2500 ms. To implement MTE-NODDI, the DWI images were acquired at three different echo times of 30, 45, and 60 ms. At each echo time, MRI protocol consisted of two shells, detailed as follows:

1. Shell One: 30 directions, five b = 0 s/mm^2 images, and diffusion weighting of b = 2000 s/mm^2
2. Shell Two: 15 directions, five b = 0 s/mm^2 images, and diffusion weighting of b = 700 s/mm^2

with gradient duration and separation δ/Δ = 4.5/11 ms for all b-values and TE's. The overall acquisition time for each mouse per imaging session was ~120 minutes.

2.4. Image processing and modelling of diffusion data

The effects of noise and imaging artifacts on the DWI images were reduced by applying a denoising method based on the random matrix theory (MRtrix3) (Veraart et al., 2016), correction of B0 inhomogeneity, and motion with TOPUP (Andersson & Sotiropoulos, 2016) in FMRIB Software Library (FSL, University of Oxford, UK). The T2-weighted and DWI acquisitions were then co-registered to a reference b=0 image. T2-weighted images were resampled to match the DWI images in AFNI (Analysis of Functional NeuroImages, National Institutes of Health, USA), and brain masks were created manually on T2-weighted images using ITK-SNAP. Mean diffusivity (MD) measures were generated from diffusion data obtained at TE = 30 ms using dtifit in FSL, which fits a diffusion tensor model at each voxel of the data that has been pre-processed. NODDI parameters were estimated for each TE session separately with the NODDI MATLAB Toolbox, and the estimated parameters were aligned to the first TE session to extract TE-independent MTE-NODDI parameters (Gong et al., 2020).

2.5. Selection of tumour regions of interest

For quantitative analysis, tumour regions of interest (ROIs) were manually defined on T2-weighted images (T2WI) using ITK-SNAP by the two authors (SK and DG) who were blinded to the other's results. The images and ROIs were presented to a consulting neurosurgeon (CSH) for approval. In our experience with the G144 model, tumour cells exhibit a spread beyond the tumour bulk, infiltrating into the peritumoural regions of corpus callosum, striatum, and cortex regions (Brooks et al., 2021). Therefore, the following ROIs were selected:

2.5.1. Tumour bulk

Regions with hyperintense signal in the ipsilateral hemisphere on the coronal T2WI were identified as tumour bulk.

2.5.2. Peritumoural margin

Regions outside the tumour bulk, where there are no T2WI changes, were defined in the ipsilateral hemisphere in three distinct anatomical regions—corpus callosum, striatum, and cortex. Given that the G144 model replicates the GBM feature of invasion along the corpus callosum, a margin region in the corpus callosum adjacent to the tumour bulk was always selected. ROIs were adjusted to exclude any confounding anatomical structures (e.g., the lateral ventricle in the striatal ROI, grey matter structures in the corpus callosum ROI, etc.). These exclusion criteria resulted in ROIs of the following sizes: corpus callosum—1 pixel (~0.182 mm) in the xy direction; striatum and cortex—up to 3 pixels (~0.550 mm). As can be seen in the representative images presented in this manuscript (Fig. 2), confounding anatomical structures such as external capsule may contaminate striatal ROIs (or corpus callosum in the cortical ROI) if extended beyond 3 pixels. In the contralateral hemisphere, ROIs equivalent to the peritumoural margins were defined as controls for comparison. Subsequently, the same ROIs were copied onto diffusion MRI images and mean values for NDI, f_{en}, ODI, and MD were extracted for quantitative analysis.

2.5.3. Histology ROI for correlation

Due to fixation and shrinkage of tissue during histology, a pixel-by-pixel comparison was not possible across the MRI and histology data sets. As such, ROIs encompassing the cortex across both hemispheres of the brain were chosen to enable an unbiased comparison between the two sets of images (Supp. Fig. 1). In animals where tumour bulk was identified in the cortex, these pixels were excluded from both the MRI and GFP images to ensure accurate correlation analysis. Opting for an ROI covering the entire cortex simplifies delineation, while simultaneously mitigating any artifacts and inaccuracies caused due to tissue fixation.

2.6. Quantification of GFP+ fluorescence from tumour cells

G144 tumour cells were transduced to constitutively express GFP using a lentiviral approach. Lentivirus carrying the GFP transgene was produced by cotransfecting with the HIV-1 packaging vector Delta8.9 and the VSVG envelope glycoprotein into 293 T cells using polyethylenimine. Virus was concentrated by ultracentrifugation (3 h, 50,000 × g, 4°C) (Brooks & Parrinello, 2017). For quantification of the fluorescence intensity from GFP+ tumour cells, mice were perfused with 4% PFA and the brain post-fixed in 4% paraformaldehyde overnight at 4°C. Two explanted brains from the MRI-imaged mice were assigned for downstream mechanistic analyses and, as such, were not included in this study, rendering them unavailable for immunofluorescence. From the remaining mice (n = 5), 50 μm vibratome sections were cover-slipped,

dried, and imaged using a Leica DMi8 Inverted microscope (Leica Microsystems, Wetzlar, Germany). Immunofluorescence images from each mouse (n = 5; 1 slice per mouse) were individually imported into ImageJ, and ROIs encompassing the entire cortex were drawn. Images were then thresholded by intensity to eliminate any signal from background, and signal intensity from GFP-positive tumour cells within the ROI was quantified as % Area under fluorescence and exported into GraphPad Prism for correlation with MRI measurements.

2.7. Statistical analysis

Statistical analysis of the data was performed using GraphPad Prism 9.0. All data are expressed as mean ± SD and were tested for normality using Shapiro-Wilk test. For the intra-animal changes between contralateral and peritumoural margin regions, paired t-tests were used to test for statistically significant difference. For the longitudinal study, we reported the data as mean ± SD of paired differences in all animals at each timepoint. In addition, Pearson correlation analysis was used to determine the correlation between MRI parameters and GFP+ fluorescence intensity from tumour cells. For all statistical tests, the significance level was $p < 0.05$.

3. RESULTS

3.1. Application of MTE-NODDI to mouse model of glioblastoma

We probed the invading margin of GBM using MTE-NODDI (Gong et al., 2020), a recent improvement of the conventional NODDI model (Zhang et al., 2012), which enables us to estimate non-T2-weighted NODDI parameters such as NDI, f_{en}, and ODI. A well-characterised G144 patient-derived xenograft mouse model, which recapitulates the hallmark feature of GBM to invade to the contralateral hemisphere along the white matter tracts of the corpus callosum (Brooks et al., 2021; Pollard et al., 2009), was used in combination with MTE-NODDI.

To assess the sensitivity of MTE-NODDI to the spread of tumour cells, GFP-labelled G144 cells were stereotactically injected into the striatum of immunocompromised mice and imaged longitudinally on the 9.4T MRI system at three timepoints after injection (4, 6, and 8 weeks). Previous studies suggest that the invasive cell fates and invasion patterns of G144 cells were different in different microenvironments of the brain (Brooks et al., 2021). In line with these observations, at the three timepoints, we used T2WI images to define hyperintense tumour bulk and peritumoural margin regions extending into the corpus callosum as a region of white matter, as well as cortex and striatum as regions of grey matter for quantitative analysis using MTE-NODDI.

Additionally, to ascertain whether MTE-NODDI provides improved sensitivity to infiltrating GBM cells, we also applied a standard diffusion tensor imaging (DTI) model to the diffusion data to calculate maps of MD. Figure 1 presents images of naïve and G144 tumour-bearing mice from a bespokeT2WI sequence, together with concomitant maps of NDI, f_{en}, ODI, and MD. The tumour bulk is readily identified as a hyperintense area on the T2WI image. The peritumoural margin regions (areas without T2 changes) surrounding the hyperintense bulk (Fig. 2) are located in the cortex, corpus callosum, and striatum.

3.2. Peritumoural margin detection using MTE-NODDI

A focus of this study was to investigate the conspicuity of the MTE-NODDI parameters to peritumoural margin regions beyond the tumour bulk, where no discernable

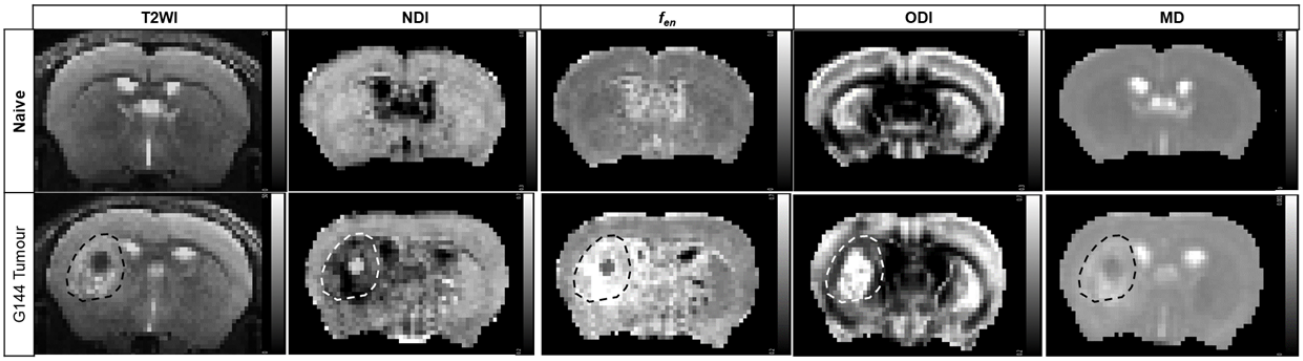

Fig. 1. Representative coronal T2WI images and maps of MTE-NODDI NDI, f_{en}, ODI, and DTI MD. Top panel: representative maps from a naive mouse at the third timepoint showing no discernable changes across both hemispheres. Bottom panel: maps from a G144 tumour-bearing mouse at the third timepoint revealing changes due to tumour cells infiltrating into the peritumoural margins. Tumour bulk identified on the T2WI is indicated by a dashed line on all maps.

changes were present in the T2WI images. At the 8-week timepoint, when the tumour is most developed, comparison of the MTE-NODDI parameters between the peritumoural margin and equivalent contralateral regions (cortex, corpus callosum, and striatum) revealed marked changes in NDI, $f_{en,}$ and ODI values outside the tumour bulk (Fig. 3, Supp. Fig. 2).

In the cortex, all three MTE-NODDI parameters NDI ($p < 0.05$), f_{en} ($p < 0.05$) and ODI ($p < 0.0005$) demonstrated clear differences in the peritumoural margin; most notably in the ODI (Fig. 3A, Supp. Fig. 2A). Similarly, in the corpus callosum margin, NDI ($p < 0.005$), ODI ($p < 0.01$), and f_{en} ($p < 0.0001$) values demonstrated excellent sensitivity of MTE-NODDI to detect tumour margin in both grey and white matter regions outside the bulk (Fig. 3B, Supp. Fig. 2B). As in the corpus callosum and cortex, peritumoural margin ROIs in the striatum had a lower ODI ($p < 0.0001$), NDI ($p < 0.005$) and higher f_{en} ($p < 0.001$) values (Fig. 3C, Supp. Fig. 2C).

Gadolinium-enhanced T1 images, alongside T2 images, are used clinically to define the area of tumour bulk (Price & Gillard, 2011). Due to the limited time during the MRI acquisition protocol, we did not acquire post-contrast T1 images. Therefore, in a separate group of tumour-bearing animals (n = 2), we compared the measured tumour volumes in our model of GBM using both gadolinium-enhanced T1-weighted and the T2WI used to identify tumour bulk. The tumour volumes were comparable (mean percentage difference = 6.7%), supporting the use of T2WI to define tumour bulk in our model (Supp. Fig. 3).

When defining the equivalent control ROIs (bulk, peritumoural margins in the cortex, striatum, and corpus callosum) in the contralateral hemisphere, there could be slight variations in ROI placement due to the tumour mass in the ipsilateral hemisphere. As such, additional controls were performed in a group of age- and strain-matched naïve mice to assess the effect of the small variation in ipsi- and contralateral ROIs (n=3) placement, due to the tumour mass in the ipsilateral striatum, on the MRI data. The MRI images from the naïve mice were co-registered to the images from the tumour-bearing mice using FMRIB Software Library (FSL, University of Oxford, UK). Subsequently, the ROIs drawn on tumour-bearing mice were superimposed onto images from the naïve mice and mean values for NDI, f_{en}, ODI, and MD were extracted for quantitative analysis. We did not note any differences in NDI, f_{en}, and ODI values between ROIs due to the tumour (Supp. Fig. 4). Therefore, there is limited contribution to the peritumoural margin data from the regional background variation in the selected ROIs.

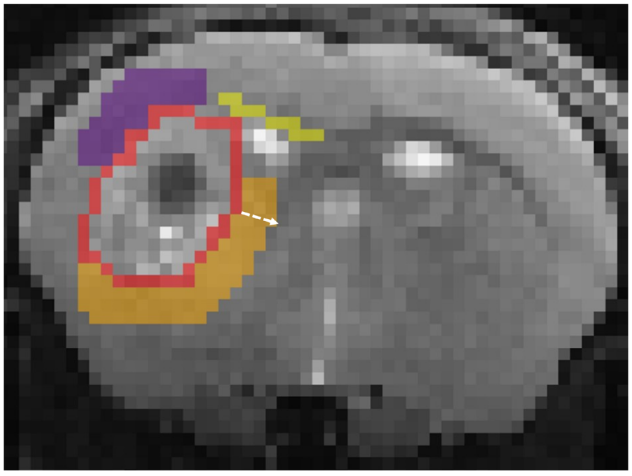

Fig. 2. Representative coronal T2WI image with defined tumour regions of interest (ROIs) for quantification of MRI parameters. For illustrative purposes, outline of tumour bulk defined on T2WI is shown in red; the peritumoural margin regions in the cortex, corpus callosum, and striatum are displayed in purple, yellow, and orange respectively. White arrow illustrates the 3-pixel extension of the ROIs around the tumour bulk.

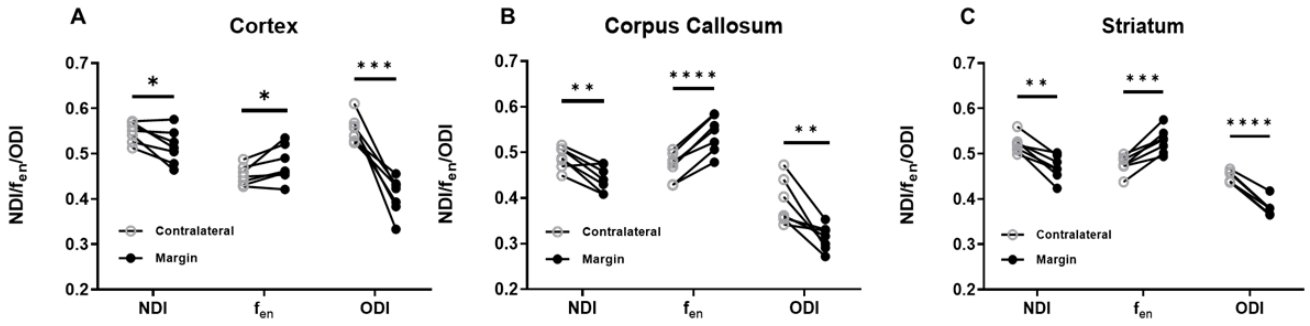

Fig. 3. Mean values of MTE-NODDI parameters extracted from the contralateral and peritumoural margin ROIs for each animal (n=7) at the 8-week timepoint. NDI, f_{en}, and ODI values from the contralateral and peritumoural margins in (A) Cortex, (B) Corpus callosum, and (C) Striatum. Each data point on the plots represents the mean value for individual mouse. Paired t-tests were used to test statistically significant differences between contralateral and peritumoural margins (*$p < 0.05$, **$p < 0.005$, ***$p < 0.001$, ****$p < 0.0005$).

3.3. Monitoring tumour invasion into peritumoural regions

We next assessed the sensitivity of MTE-NODDI parameters to tumour-induced microstructure changes (NDI, f_{en}, and ODI) at all three imaging timepoints (4, 6, and 8 weeks) across three anatomical regions (Fig. 4A). MTE-NODDI parameters measured from ROIs drawn at the respective timepoints were clearly sensitive to tumour evolution over the 4-week imaging period. These peritumoural margin changes were most notable from the 6-week time point onwards. For instance, beginning at the 6-week timepoint, all MTE-NODDI parameters in the striatum exhibited sensitivity to tumour-induced pathology, with decreased NDI ($p < 0.005$), and ODI ($p < 0.05$), while the f_{en} ($p < 0.005$) was increased (Fig. 4Ai-iii).

3.4. Increased sensitivity of MTE-NODDI to invading tumour margin compared with MD

Our subsequent aim was to evaluate whether MTE-NODDI was more sensitive to tumour-induced changes than the established DWI measure of MD. We observed that differences in NDI, $f_{en,}$ and ODI values were consistently higher than MD values, indicating that MTE-NODDI offers increased sensitivity to microstructural changes in the peritumoural margin as the tumour invades normal brain tissue. More specifically, we detected increases in striatal ODI as early as week 4 without any associated changes in MD (Fig. 4B). This heightened sensitivity was also observed at 6 and 8 weeks in the cortex, as well as at 8 weeks in the corpus callosum, thereby providing strong evidence for the increased conspicuity of MTE-NODDI to tumour-induced microstructural changes in regions without MD or T2WI changes. Importantly we did not observe any changes (NDI, $f_{en,}$ ODI, and MD) in control age-matched and strain-matched naïve animals (n=3) over the 3 timepoints (Supp. Fig. 5). Taken together, this provides evidence that MTE-NODDI parameters are sensitive to tumour-induced microstructural pathology as it invades into regions outside the tumour bulk.

3.5. Invading tumour cells correlate with NDI and f_{en}

Finally, we sought to examine the effectiveness of MTE-NODDI as an *in vivo* imaging marker to detect invading tumour cells in the tumour margin, by comparing fluorescence (% area) from GFP+ tumour cells measured using

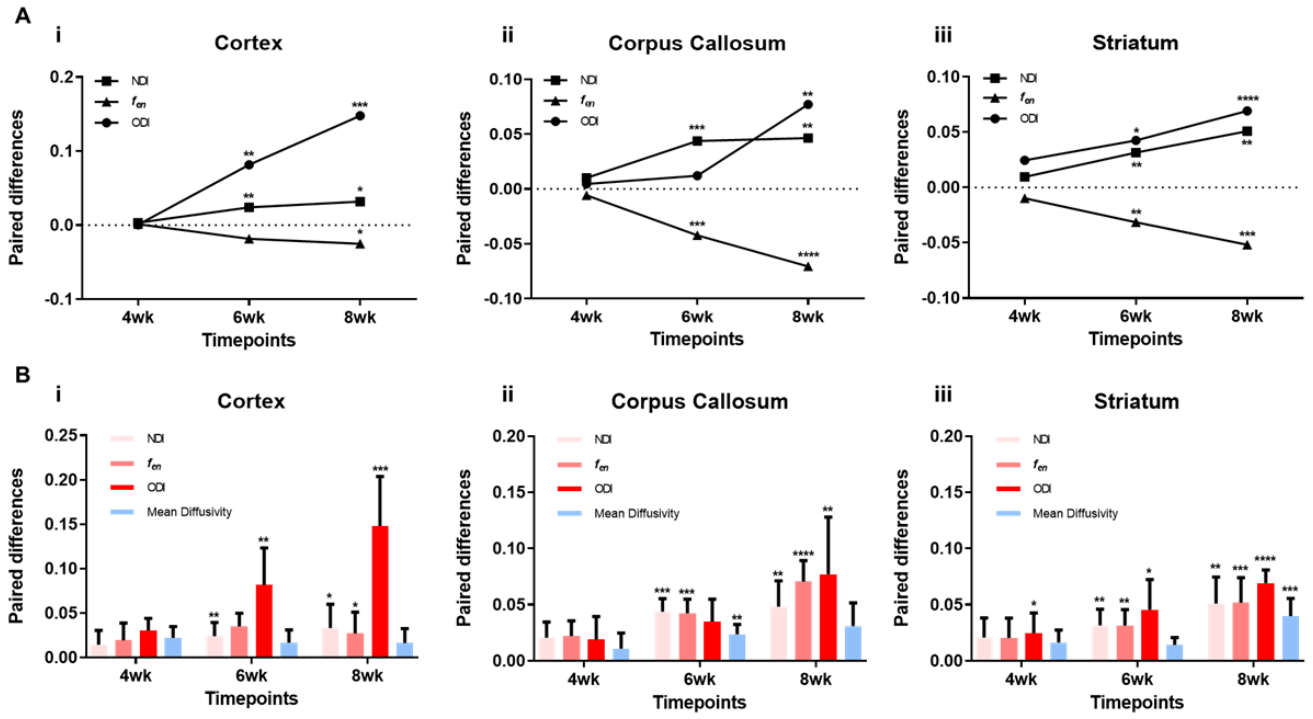

Fig. 4. MTE-NODDI and MD changes over time with developing tumour. (A) Paired differences (Contralateral–Peritumoural Margin) of NDI, f_{en}, and ODI at 4 wk, 6 wk, and 8 wk timepoints in (i) Cortex, (ii) Corpus callosum, and (iii) Striatum. Each data point in the plot represents the mean of paired differences from all animals (n=7). (B) Paired differences (Contralateral–Peritumoural Margin) of NDI, f_{en}, ODI, and MD at 4 wk, 6 wk, and 8 wk timepoints in (i) Cortex, (ii) Corpus callosum, and (iii) Striatum. Barplots represent means of paired differences from all animals (n=7), where MTE-NODDI parameters are shown in red, and DTI MD is plotted in blue for illustrative purposes. Paired t-tests were used to test statistically significant differences between contralateral and peritumoural margins (*$p < 0.05$, **$p < 0.005$, ***$p < 0.001$, ****$p < 0.0005$).

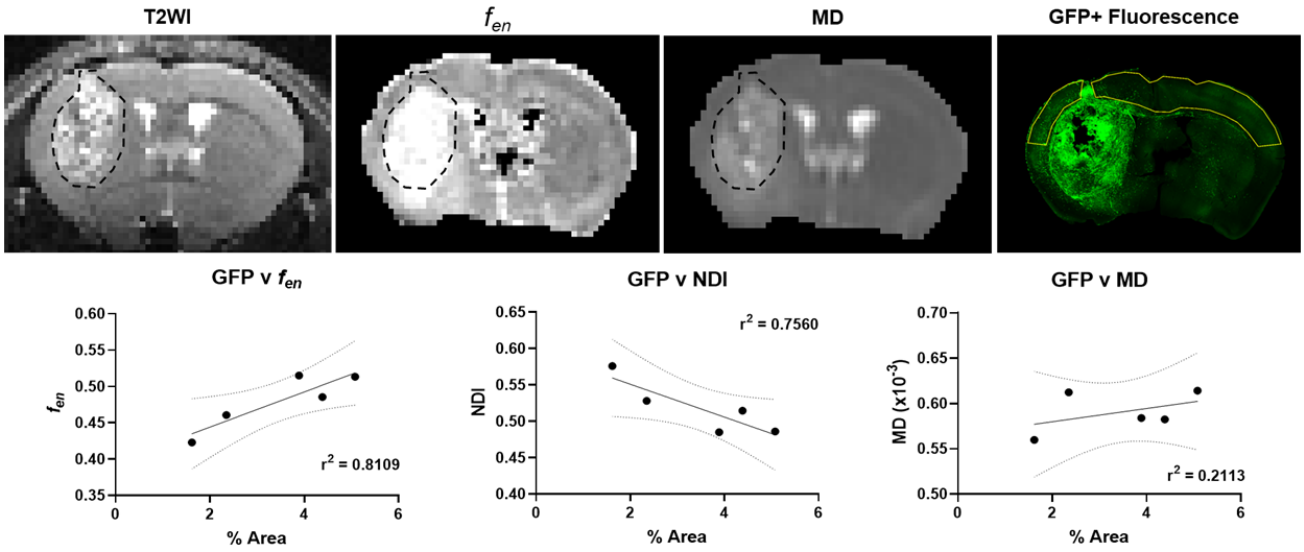

Fig. 5. MTE-NODDI values in the cortex correlated with GFP+ fluorescence from tumour mice. Top Panel: Representative T2WI image, f_{en} map, MD map, and GFP+ histological image from a G144 tumour mouse. Tumour bulk as identified on the T2WI is indicated by a dashed black line. The cortical ROI used for correlation is indicated in solid yellow. Bottom Panel: Correlation of f_{en}, NDI, and MD to GFP+ fluorescence. MTE-NODDI and MD values were extracted from a region drawn in the cortex across both hemispheres. GFP+ fluorescence is calculated as % Area under fluorescence from an equivalent cortical region drawn on immunohistological images (n=5). Pearson's correlation coefficient was used to investigate a possible correlation (r^2 values reported on respective plots).

immunohistological images with the MRI parameters (Fig. 5). Importantly, the GFP+ cell distribution observed in the immunohistological images confirmed tumour cell infiltration into all three anatomical brain regions tested (cortex, corpus collosum, and striatum) (Fig. 5; top panel). MTE-NODDI values in the cortex show that both f_{en} ($R^2 = 0.81$ and $p < 0.05$) and NDI ($R^2 = 0.76$ and $p < 0.05$) demonstrated strong correlations with GFP+ fluorescence, with MD displaying no such correlation ($R^2 = 0.21$ and $p = 0.44$). As such, we observe improved specificity of the technique over MD for detecting tumour-induced pathology correlating with migrating tumour cells. To expand upon these findings, we analysed an additional 9 GFP+ immunohistological sections from the rostral edge of the tumour bulk. We did not find any correlations between GFP+ fluorescence and the MRI parameters. However, in this anterior region, the cell count was eight times lower (0.28%) compared to the central, more cellularly dense portion of the tumour (1.56%) ($p = 0.05$) (Supp. Fig. 6). We believe the lack of correlation is due to the scarcity of cells thus limiting sensitivity, as most likely beyond the limits of detection in the regions at the anterior boundary of the tumour.

4. DISCUSSION

Precise tumour margin delineation in GBM remains a profound challenge due to its highly invasive nature and diffuse pattern of tumour cell migration into healthy brain regions. Here, we report the first application of MTE-NODDI to non-invasively detect infiltrating cells in a patient-derived xenograft mouse model of GBM in regions outside the tumour bulk. We demonstrate that MTE-NODDI detected tumour-induced pathology in margin regions without T2 or MRI-diffusion changes. Furthermore, MTE-NODDI parameters correlated with immunohistological measure of tumour cell infiltration. These findings highlight the sensitivity of MTE-NODDI to invading tumour cells and associated pathology, suggesting its utility in imaging peritumoural margins of GBM.

Traditionally, NODDI was developed to provide microstructural information that is more specific than DTI by separating the diffusion signal into intra-neurite, extra-neurite, and free water fractions (Zhang et al., 2012). The NODDI model, generates two key variables, neurite density index (NDI) and orientation dispersion index (ODI). Additionally, free water fraction (f_{iso}) and extra-neurite volume fraction (f_{en}) can be derived when studying the influence of CSF and extra-neurite structures (like soma, glial cells, invading tumour cells etc.) respectively. The technique is suitable for both grey and white matter (Winston et al., 2014) and has been valuable in evaluating axonal/dendritic degeneration and fiber orientation in various neurological diseases, such as Alzheimer's disease (Colgan et al., 2016; Fu et al., 2020; Parker et al., 2018), Parkinson's disease (Kamagata et al., 2017; Mitchell et al., 2019), MS (Schneider et al., 2017; Spano et al., 2018), ischemic stroke (Mastropietro et al., 2019; Z. Wang

et al., 2019), and epilepsy (Sone et al., 2018; Winston et al., 2014). Importantly, NODDI has also been successfully applied to brain tumours (Kamiya et al., 2020; Sanvito et al., 2021), primarily in grading (Figini et al., 2018; Zhao et al., 2018) but also to differentiate primary GBM tumour bulk from brain metastases (Kadota et al., 2020; Mao et al., 2020; Wen et al., 2015), as well as vasogenic oedema from tumour infiltration (Caverzasi et al., 2016; Chong et al., 2021; Masjoodi et al., 2018). However, there are no reports investigating the role of NODDI in detecting infiltrating tumour margin beyond regions with T1 or T2 abnormalities.

Outside the bulk of the tumour, in the hard-to-detect peritumoural margin regions, we observe marked changes in the MTE-NODDI parameters. Several studies have examined the association between mean diffusivity (MD), also known as the apparent diffusion coefficient (ADC), and tumour cellularity in GBM. Some studies have reported a decrease in MD with tumour progression and a negative correlation between MD and tumour cellularity in these regions (Chang et al., 2017; Chenevert et al., 2000; Kono et al., 2001; Sugahara et al., 1999), while others have found MD maps less useful or reported inverse findings (Berro et al., 2019; Price et al., 2006; Sadeghi et al., 2008). When we compared our measurements of MTE-NODDI changes to the more established MD, we observed that MTE-NODDI has a greater sensitivity to infiltrating tumour cells. In our mouse model, we observed an increase in MD values in the peritumoural margins, suggesting the influence of other factors such as peritumoural oedema (Lemercier et al., 2014). Given that the hyperintense regions in T2WI and contrast-enhancing regions in T1-weighted imaging were comparable, this finding suggests that the model does not exhibit oedema. The absence of oedema is reinforced by the lack of hyperintense signals on T2WI outside the boundaries of the contrast-enhancing region. Our findings suggest that infiltrating tumour cells, perhaps coupled with microstructural changes induced by cell invasion, can be detected by MTE-NODDI. As such, MTE-NODDI with its improved sensitivity may provide a tool for detecting tumour invasion into the peritumoural margin regions in GBM.

In terms of tumour growth, MTE-NODDI parameters readily detected tumour evolution (4–8 weeks) as the tumour cells infiltrate out from the bulk into the peritumoural margins. NODDI has been previously used to investigate the relationship between disease progression and WM-changes in traumatic brain injury (Palacios et al., 2020) stroke (Mastropietro et al., 2019), athletic concussion (Churchill et al., 2019), and schizophrenia (Kraguljac et al., 2021). Taken together with our data, we anticipate that MTE-NODDI could be valuable in evaluating longitudinal microstructural changes in the brain induced by infiltrating tumour cells.

Previous studies have noted increased ODI in the tumour bulk, likely due to disruption of neuronal structural integrity (Masjoodi et al., 2018; Onishi et al., 2022). Conversely, we observe a decrease in ODI in the margin regions, which may suggest increased microstructural directionality due to invading GBM tumour cells. Recently, invasion in GBM has been described as having multiple traits of neuronal development, including formation of neurogliomal synapses that simulate 'neurite-like' tumour microtubes (Venkataramani et al., 2019), alongside increases in solid stress and compression (Seano et al., 2019), which may lead to a decrease in dispersion of neurites and consequently lower ODI. Thus, it is conceivable, that in the peritumoural margin regions, tumour cell infiltration may contribute to the observed decrease in ODI values.

Our observed increase in f_{en} values may be driven by infiltrating tumour cells within the extra-neurite spaces in the peritumoural margin. When patient-derived glioma cells are implanted into rodent brains, a substantial amount of these cells migrate along the vascular surfaces to invade the healthy brain (Brooks & Parrinello, 2017; Cuddapah et al., 2014). These infiltrating tumour cells can be associated with the NODDI extra-neurite compartment (f_{en}), in the same fashion as microglia, glial cells, and ependymal cells (Caverzasi et al., 2016; Kadota et al., 2020). Previously, it has been demonstrated that microglial density is a key contributor to measures of NODDI extra-neurite compartment (f_{en}) (Yi et al., 2019). Similarly, as GBM cells infiltrate into the peritumoural margins with tumour development, there is a corresponding increase in f_{en} values supporting the contribution of GBM cells to an increase in the measured extra-neurite compartment index (f_{en}).

We also observed lower NDI in the peritumoural regions, which may be due to a relative decrease in intra-neurite volume fraction caused by infiltrating tumour cells in the extra-neurite spaces, causing a shift in diffusion property of the tissue from a restricted intra-neurite compartment towards a hindered extra-neurite compartment (Kadota et al., 2020; Yi et al., 2019). Therefore, as tumour cells invade into the margin, this may reduce the intra-neurite volume fraction leading to a decrease NDI. Previous studies featuring use of NODDI in the glioma bulk (Jin et al., 2020; Kadota et al., 2020; Onishi et al., 2022; Zhao et al., 2018) have shown a decreased NDI, suggesting possible neuronal loss and fibre disruption, yet this may also reflect the increased cellular density in the tumour bulk, as observed in the margin of our study.

These observations were further explored by investigating the relationship between MTE-NODDI parameters and

infiltrating tumour cells (GFP+ fluorescence). In our tumour model, f_{en} and NDI correlated well with GFP+ fluorescence. NODDI has been previously used to investigate microstructural alterations in an Alzheimer's mouse model of tau pathology, where NDI values correlated with disease burden (Colgan et al., 2016). Our results indicate that infiltrating tumour cells may account for the changes in MTE-NODDI parameters, although this does not exclude additional tumour-induced microstructural changes, such as pathological demyelination (Brooks et al., 2021; J. Wang et al., 2018), and water retention in the surrounding tissue (Onishi et al., 2022; Wen et al., 2015).

As this was a proof-of-concept study, there is an opportunity for building on the experimental design. The potential presence of tumour cells within the contralateral control hemisphere may result in an underestimation of the observed differences between the peritumoural and contralateral control ROIs. Incorporating a baseline scan to establish control values before the onset of disease may contribute to the ability of MTE-NODDI to detect peritumoural invasion. There is also an opportunity to further disentangle the observed differences in MTE-NODDI metrics resulting from infiltrating tumour cells and those caused due to pathological microstructural changes such as demyelination, angiogenesis, alterations to the extra cellular matrix, and other deformations in the brain due to tumour-growth (Brooks et al., 2022; Lathia et al., 2011; Seano et al., 2019). Furthermore, a multi-timepoint acquisition of MRI data with matched multi-slice histology at each timepoint would enable a comprehensive understanding of the specificity of MTE-NODDI metrics to infiltrating tumour cells across the entire brain. Investigating the histological images from the anterior portion of the tumour did not yield significant findings, which we believe is likely due to the limited number of invading tumour cells in that region (8 times lower compared to the central core of the tumour). In addition, the relatively small size of the tumour compared to the MRI slice thickness may result in small or subtle areas of tumour infiltration to be missed or averaged out in the imaging data, reducing the ability to precisely correlate the MRI findings with the histological data. Future studies should consider using reduced imaging slice thickness and multiple histological sections spanning the entire tumour length to further establish specificity of the technique for detecting migrating tumour cells. Additionally, establishing direct co-registration between MRI images and histological sections could facilitate a pixel-by-pixel analysis of the MRI signal, which was not possible in this study. Moreover, in the present study, we define the tumour bulk and peritumoural margin regions based on T2-weighted images. To better align with imaging protocols commonly employed in clinical settings, a multi-parametric acquisition that includes contrast-enhanced T1-weighted images and FLAIR imaging for ROI delineation, along with T2 mapping for quantitative analysis, would be more suitable. In terms of other methods, the ongoing development of imaging techniques (Laack et al., 2021; Laprie et al., 2024; Ramesh et al., 2022) suggests that a multiparametric imaging approach may contribute to understanding this complex and challenging brain tumour type.

5. CONCLUSIONS

In conclusion, this study establishes the clear value of MTE-NODDI in detecting infiltrating GBM cells in the peritumoural margin outside regions of T2WI and MD abnormalities. MTE-NODDI parameters NDI, f_{en}, and ODI all change markedly in areas with tumour cell infiltration and associated microstructural alterations. Moreover, the correlations between immunohistological measure of tumour cells and MTE-NODDI parameters provide evidence of sensitivity of MTE-NODDI to low numbers of infiltrating tumour cells. Mounting evidence shows improved survival with extending resection into the non-contrast enhancing regions (De Leeuw & Vogelbaum, 2019; Jackson et al., 2020). Therefore, findings from this study suggest that MTE-NODDI could be used to improve tumour margin detection and aid neurosurgeons in maximising the extent of surgical resection to achieve better survival and quality-of-life outcomes.

DATA AND CODE AVAILABILITY

The data generated in this study are available upon reasonable request from the corresponding author.

AUTHOR CONTRIBUTIONS

S.R.K.: Data curation, Formal analysis, Investigation, Methodology, Visualisation, and Writing—original draft. D.G.: Data curation, Formal analysis, Investigation, Visualisation, and Writing—review & editing. D.T.: Data curation, Methodology, Software, and Writing—review & editing. L.J.B.: Methodology, Writing—review & editing. T.G.: Methodology, Validation, and Software. A.C.S.J.: Formal analysis, Visualisation, and Writing—review & editing. C.S.H.: Formal analysis, Writing—review & editing. M.C.: Formal analysis, Writing—review & editing. T.L.K.: Formal analysis, Writing—review & editing. J.A.W.: Methodology, Writing—review & editing. D.J.S.: Formal analysis, Writing—review & editing. L. T.: Formal analysis, Writing—review & editing. V.S.: Formal analysis, Supervision, Funding acquisition,

and Writing—review & editing. S.M.: Formal analysis, Supervision, Funding acquisition, and Writing—review & editing. H.Z.: Metholodology, Validation, and Software. S.P.: Conceptualisation, Formal analysis, Supervision, Funding acquisition, and Writing—review & editing. M.F.L.: Conceptualisation, Formal analysis, Supervision, Funding acquisition, and Writing—original draft.

DECLARATION OF COMPETING INTEREST

The authors declare that they have no competing interests.

ACKNOWLEDGEMENTS

S.R.K. was supported by The Edinburgh-UCL Cancer Research UK (CRUK) Brain Tumour Centre of Excellence award [C7893/A27590]. This work was supported in part by The Oli Hilsdon Foundation through The Brain Tumour Charity, grant number (GN-000595), in connection with the program "Mapping the spatio-temporal heterogeneity of glioblastoma invasion" (D.G., M.C., A.C.S.J.). D.T.'s salary was supported by CRUK City of London (CoL) Centre. A.C.S.J. is supported by the Eric and Wendy Schmidt AI in Science Postdoctoral Fellowship, a Schmidt Futures program. L.J.B. was funded from Cancer Research UK (CRUK) RadNet in the form of an early career fellowship. C.S.H. was supported by a CRUK Pioneer Award (C70568/A29787), an AMS Starter Grant (SGL021\1034), a National Brain Appeal Innovation Award (NBA/NSG/BTB), and UCLH BRC NIHR funding. J.A.W. is supported by the Wellcome Trust (225345/Z/22/Z). VS was supported by the Engineering and Physical Sciences Research Council (EP/N014529/1). S.M. was supported by the UK Medical Research Council. S.P. was supported by CRUK (awards C55501/A21203 and 7550844). M.F.L. was supported by the Rosetrees Trust and the John Black Charitable Foundation (grant no. A2200). The authors would like to thank Shereen Nizari for their help in data acquisition.

SUPPLEMENTARY MATERIALS

Supplementary material for this article is available with the online version here: https://doi.org/10.1162/imag_a_00472.

REFERENCES

Andersson, J. L. R., & Sotiropoulos, S. N. (2016). An integrated approach to correction for off-resonance effects and subject movement in diffusion MR imaging. *NeuroImage*, *125*, 1063–1078. https://doi.org/10.1016/J.NEUROIMAGE.2015.10.019

Basser, P. J., Mattiello, J., & LeBihan, D. (1994). MR diffusion tensor spectroscopy and imaging. *Biophysical Journal*, *66*(1), 259–267. https://doi.org/10.1016/S0006-3495(94)80775-1

Berro, D. H., Collet, S., Constans, J. M., Barré, L., Derlon, J. M., Emery, E., Guillamo, J. S., & Valable, S. (2019). Comparison between MRI-derived ADC maps and 18FLT-PET in pre-operative glioblastoma. *Journal of Neuroradiology*, *46*(6), 359–366. https://doi.org/10.1016/J.NEURAD.2019.05.011

Bouyagoub, S., Dowell, N., Hurley, S. A., Wood, T. C., & Cercignani, M. (2016). Overestimation of CSF fraction in NODDI: Possible correction techniques and the effect on neurite density and orientation dispersion measures. *24th Annual Meeting & Exhibition*. *Archive.Ismrm.Org*. https://archive.ismrm.org/2016/0007.html

Brooks, L. J., Clements, M. P., Burden, J. J., Kocher, D., Richards, L., Devesa, S. C., Zakka, L., Woodberry, M., Ellis, M., Jaunmuktane, Z., Brandner, S., Morrison, G., Pollard, S. M., Dirks, P. B., Marguerat, S., & Parrinello, S. (2021). The white matter is a pro-differentiative niche for glioblastoma. *Nature Communications*, *12*(1), 1–14. https://doi.org/10.1038/s41467-021-22225-w

Brooks, L. J., & Parrinello, S. (2017). Vascular regulation of glioma stem-like cells: A balancing act. *Current Opinion in Neurobiology*, *47*, 8–15. https://doi.org/10.1016/J.CONB.2017.06.008

Brooks, L. J., Simpson Ragdale, H., Hill, C. S., Clements, M., & Parrinello, S. (2022). Injury programs shape glioblastoma. *Trends in Neurosciences*, *45*(11), 865–876. https://doi.org/10.1016/J.TINS.2022.08.006

Caverzasi, E., Papinutto, N., Castellano, A., Zhu, A. H., Scifo, P., Riva, M., Bello, L., Falini, A., Bharatha, A., & Henry, R. G. (2016). Neurite orientation dispersion and density imaging color maps to characterize brain diffusion in neurologic disorders. *Journal of Neuroimaging: Official Journal of the American Society of Neuroimaging*, *26*(5), 494–498. https://doi.org/10.1111/JON.12359

Chamberlain, M. C. (2011). Bevacizumab for the treatment of recurrent glioblastoma. Clinical medicine insights. *Oncology*, *5*(5), 117. https://doi.org/10.4137/CMO.S7232

Chang, P. D., Chow, D. S., Yang, P. H., Filippi, C. G., & Lignelli, A. (2017). Predicting glioblastoma recurrence by early changes in the apparent diffusion coefficient value and signal intensity on FLAIR images. *American Journal of Roentgenology*, *208*(1), 57–65. https://doi.org/10.2214/AJR.16.16234

Chenevert, T. L., Stegman, L. D., Taylor, J. M. G., Robertson, P. L., Greenberg, H. S., Rehemtulla, A., & Ross, B. D. (2000). Diffusion magnetic resonance imaging: An early surrogate marker of therapeutic efficacy in brain tumors. *Journal of the National Cancer Institute*, *92*(24), 2029–2036. https://academic.oup.com/jnci/article-abstract/92/24/2029/2633587

Chong, S. T., Liu, X., Kao, H. W., Lin, C. Y. E., Hsu, C. C. H., Kung, Y. C., Kuo, K. T., Huang, C. C., Lo, C. Y. Z., Li, Y., Zhao, G., & Lin, C. P. (2021). Exploring peritumoral neural tracts by using neurite orientation dispersion and density imaging. *Frontiers in Neuroscience*, *15*, 702353. https://doi.org/10.3389/FNINS.2021.702353

Churchill, N. W., Caverzasi, E., Graham, S. J., Hutchison, M. G., & Schweizer, T. A. (2019). White matter during concussion recovery: Comparing diffusion tensor imaging (DTI) and neurite orientation dispersion and density imaging (NODDI). *Human Brain Mapping*, *40*(6), 1908. https://doi.org/10.1002/HBM.24500

Claes, A., Idema, A. J., & Wesseling, P. (2007). Diffuse glioma growth: A guerilla war. *Acta Neuropathologica*, *114*(5), 443–458. https://doi.org/10.1007/S00401-007-0293-7

Colgan, N., Siow, B., O'Callaghan, J. M., Harrison, I. F., Wells, J. A., Holmes, H. E., Ismail, O., Richardson, S., Alexander, D. C., Collins, E. C., Fisher, E. M., Johnson, R., Schwarz, A. J., Ahmed, Z., O'Neill, M. J., Murray, T. K., Zhang, H., & Lythgoe, M. F. (2016). Application of neurite orientation dispersion and density imaging (NODDI) to a tau pathology model of Alzheimer's disease. *NeuroImage*, *125*, 739–744. https://doi.org/10.1016/J.NEUROIMAGE.2015.10.043

Cox, S. R., Ritchie, S. J., Tucker-Drob, E. M., Liewald, D. C., Hagenaars, S. P., Davies, G., Wardlaw, J. M., Gale, C. R., Bastin, M. E., & Deary, I. J. (2016). Ageing and brain white matter structure in 3,513 UK Biobank participants. *Nature Communications*, *7*(1), 1–13. https://doi.org/10.1038/ncomms13629

Cuddapah, V. A., Robel, S., Watkins, S., & Sontheimer, H. (2014). A neurocentric perspective on glioma invasion. *Nature Reviews. Neuroscience*, *15*(7), 455–465. https://doi.org/10.1038/NRN3765

De Bonis, P., Anile, C., Pompucci, A., Fiorentino, A., Balducci, M., Chiesa, S., Lauriola, L., Maira, G., & Mangiola, A. (2013). The influence of surgery on recurrence pattern of glioblastoma. *Clinical Neurology and Neurosurgery*, *115*(1), 37–43. https://doi.org/10.1016/J.CLINEURO.2012.04.005

De Leeuw, C. N., & Vogelbaum, M. A. (2019). Supratotal resection in glioma: A systematic review. *Neuro-Oncology*, *21*(2), 179–188. https://doi.org/10.1093/NEUONC/NOY166

Figini, M., Riva, M., Graham, M., Castelli, G., Fernandes, B., Grimaldi, M., Baselli, G., Pessina, F., Bello, L., Zhang, H., & Bizzi, A. (2018). Prediction of isocitrate dehydrogenase genotype in brain gliomas with MRI: Single-shell versus multishell diffusion models. *Radiology*, *289*. https://doi.org/10.1148/radiol.2018180054

Fu, X., Shrestha, S., Sun, M., Wu, Q., Luo, Y., Zhang, X., Yin, J., & Ni, H. (2020). Microstructural white matter alterations in mild cognitive impairment and Alzheimer's disease: Study based on neurite orientation dispersion and density imaging (NODDI). *Clinical Neuroradiology*, *30*(3), 569–579. https://doi.org/10.1007/S00062-019-00805-0

Gong, T., Tong, Q., He, H., Sun, Y., Zhong, J., & Zhang, H. (2020). MTE-NODDI: Multi-TE NODDI for disentangling non-T2-weighted signal fractions from compartment-specific T2 relaxation times. *NeuroImage*, *217*, 116906. https://doi.org/10.1016/J.NEUROIMAGE.2020.116906

Hadjipanayis, C. G., Widhalm, G., & Stummer, W. (2015). What is the surgical benefit of utilizing 5-aminolevulinic acid for fluorescence-guided surgery of malignant gliomas? *Neurosurgery*, *77*(5), 663–673. https://doi.org/10.1227/NEU.0000000000000929

Jackson, C., Choi, J., Khalafallah, A. M., Price, C., Bettegowda, C., Lim, M., Gallia, G., Weingart, J., Brem, H., & Mukherjee, D. (2020). A systematic review and meta-analysis of supratotal versus gross total resection for glioblastoma. *Journal of Neuro-Oncology*, *148*(3), 419–431. https://doi.org/10.1007/S11060-020-03556-Y

Jin, Y., Randall, J. W., Elhalawani, H., Al Feghali, K. A., Elliott, A. M., Anderson, B. M., Lacerda, L., Tran, B. L., Mohamed, A. S., Brock, K. K., Fuller, C. D., & Chung, C. (2020). Detection of glioblastoma subclinical recurrence using serial diffusion tensor imaging. *Cancers*, *12*(3), 568. https://doi.org/10.3390/CANCERS12030568

Kadota, Y., Hirai, T., Azuma, M., Hattori, Y., Khant, Z. A., Hori, M., Saito, K., Yokogami, K., & Takeshima, H. (2020). Differentiation between glioblastoma and solitary brain metastasis using neurite orientation dispersion and density imaging. *Journal of Neuroradiology*, *47*(3), 197–202. https://doi.org/10.1016/J.NEURAD.2018.10.005

Kamagata, K., Zalesky, A., Hatano, T., Ueda, R., Di Biase, M. A., Okuzumi, A., Shimoji, K., Hori, M., Caeyenberghs, K., Pantelis, C., Hattori, N., & Aoki, S. (2017). Gray matter abnormalities in idiopathic Parkinson's disease: Evaluation by diffusional kurtosis imaging and neurite orientation dispersion and density imaging. *Human Brain Mapping*, *38*(7), 3704–3722. https://doi.org/10.1002/HBM.23628

Kamiya, K., Hori, M., & Aoki, S. (2020). NODDI in clinical research. *Journal of Neuroscience Methods*, *346*, 108908. https://doi.org/10.1016/J.JNEUMETH.2020.108908

Kim, M. M., Sun, Y., Aryal, M. P., Parmar, H. A., Piert, M., Rosen, B., Mayo, C. S., Balter, J. M., Schipper, M., Gabel, N., Briceño, E. M., You, D., Heth, J., Al-Holou, W., Umemura, Y., Leung, D., Junck, L., Wahl, D. R., Lawrence, T. S., & Cao, Y. (2021). A phase 2 study of dose-intensified chemoradiation using biologically based target volume definition in patients with newly diagnosed glioblastoma. *International Journal of Radiation Oncology, Biology, Physics*, *110*(3), 792–803. https://doi.org/10.1016/j.ijrobp.2021.01.033

Kono, K., Inoue, Y., Nakayama, K., Shakudo, M., Morino, M., Ohata, K., Wakasa, K., & Yamada, R. (2001). The role of diffusion-weighted imaging in patients with brain tumors. *AJNR: American Journal of Neuroradiology*, *22*(6), 1081. https://doi.org/10.18535/jmscr/v6i2.95

Kraguljac, N. V., Monroe, W. S., Anthony, T., Jindal, R. D., Hill, H., & Lahti, A. C. (2021). Neurite orientation dispersion and density imaging (NODDI) and duration of untreated psychosis in antipsychotic medication-naïve first episode psychosis patients. *Neuroimage: Reports*, *1*(1), 100005. https://doi.org/10.1016/J.YNIRP.2021.100005

Kubben, P. L., ter Meulen, K. J., Schijns, O. E. M. G., ter Laak-Poort, M. P., van Overbeeke, J. J., & van Santbrink, H. (2011). Intraoperative MRI-guided resection of glioblastoma multiforme: A systematic review. *The Lancet Oncology*, *12*(11), 1062–1070. https://doi.org/10.1016/S1470-2045(11)70130-9

Laack, N. N., Pafundi, D., Anderson, S. K., Kaufmann, T., Lowe, V., Hunt, C., Vogen, D., Yan, E., Sarkaria, J., Brown, P., Kizilbash, S., Uhm, J., Ruff, M., Zakhary, M., Zhang, Y., Seaberg, M., Wan Chan Tseung, H. S., Kabat, B., Kemp, B., & Brinkmann, D. (2021). Initial results of a phase 2 trial of 18F-DOPA PET-guided dose-escalated radiation therapy for glioblastoma. *International Journal of Radiation Oncology Biology Physics*, *110*(5), 1383–1395. https://doi.org/10.1016/j.ijrobp.2021.03.032

Lampinen, B., Szczepankiewicz, F., Novén, M., van Westen, D., Hansson, O., Englund, E., Mårtensson, J., Westin, C. F., & Nilsson, M. (2019). Searching for the neurite density with diffusion MRI: Challenges for biophysical modeling. *Human Brain Mapping*, *40*(8), 2529–2545. https://doi.org/10.1002/HBM.24542

Lasocki, A., & Gaillard, F. (2019). Non-contrast-enhancing tumor: A new frontier in glioblastoma research. *AJNR: American Journal of Neuroradiology*, *40*(5), 758. https://doi.org/10.3174/AJNR.A6025

Lathia, J. D., Heddleston, J. M., Venere, M., & Rich, J. N. (2011). Cell stem cell minireview deadly teamwork: Neural cancer stem cells and the tumor microenvironment. *Stem Cell*, *8*, 482–485. https://doi.org/10.1016/j.stem.2011.04.013

Le Bihan, D. (2014). Diffusion MRI: What water tells us about the brain. *EMBO Molecular Medicine*, *6*(5), 569–573. https://doi.org/10.1002/EMMM.201404055

Laprie, A., Noel, G., Chaltiel, L., Truc, G., Sunyach, M.-P., Charissoux, M., Magne, N., Auberdiac, P., Biau, J., Ken, S., Tensaouti, F., Khalifa, J., Sidibe, I., Roux, F.-E., Vieillevigne, L., Catalaa, I., Boetto, S., Uro-Coste, E., Supiot, S., … Cohen-Jonathan-Moyal, E. (2024). Randomized phase III trial of metabolic imaging-guided dose escalation of radio-chemotherapy in patients with newly diagnosed glioblastoma (SPECTRO GLIO trial). *Neuro-Oncology*, *26*(1), 153–163. https://doi.org/10.1093/neuonc/noad119

Lemercier, P., Maya, S. P., Patrie, J. T., Flors, L., & Leiva-Salinas, C. (2014). Gradient of apparent diffusion coefficient values in peritumoral edema helps in differentiation of glioblastoma from solitary metastatic lesions. *American Journal of Roentgenology*, *203*(1), 163–169. https://doi.org/10.2214/AJR.13.11186

Maier, S. E., Sun, Y., & Mulkern, R. V. (2010). Diffusion imaging of brain tumors. *NMR in Biomedicine*, *23*(7), 849. https://doi.org/10.1002/NBM.1544

Mao, J., Zeng, W., Zhang, Q., Yang, Z., Yan, X., Zhang, H., Wang, M., Yang, G., Zhou, M., & Shen, J. (2020). Differentiation between high-grade gliomas and solitary brain metastases: A comparison of five diffusion-weighted MRI models. *BMC Medical Imaging*, *20*(1), 1–11. https://doi.org/10.1186/S12880-020-00524-W

Masjoodi, S., Hashemi, H., Oghabian, M. A., & Sharifi, G. (2018). Differentiation of edematous, tumoral and normal areas of brain using diffusion tensor and neurite orientation dispersion and density imaging. *Journal of Biomedical Physics & Engineering*, *8*(3), 251. https://doi.org/10.31661/jbpe.v0i0.874

Mastropietro, A., Rizzo, G., Fontana, L., Figini, M., Bernardini, B., Straffi, L., Marcheselli, S., Ghirmai, S., Nuzzi, N. P., Malosio, M. L., & Grimaldi, M. (2019). Microstructural characterization of corticospinal tract in subacute and chronic stroke patients with distal lesions by means of advanced diffusion MRI. *Neuroradiology*, *61*(9), 1033. https://doi.org/10.1007/S00234-019-02249-2

Maximov, I. I., Tonoyan, A. S., & Pronin, I. N. (2017). Differentiation of glioma malignancy grade using diffusion MRI. *Physica Medica: PM: An International Journal Devoted to the Applications of Physics to Medicine and Biology: Official Journal of the Italian Association of Biomedical Physics (AIFB)*, *40*, 24–32. https://doi.org/10.1016/J.EJMP.2017.07.002

Miller, K. D., Ostrom, Q. T., Kruchko, C., Patil, N., Tihan, T., Cioffi, G., Fuchs, H. E., Waite, K. A., Jemal, A., Siegel, R. L., & Barnholtz-Sloan, J. S. (2021). Brain and other central nervous system tumor statistics, 2021. *CA: A Cancer Journal for Clinicians*, *71*(5), 381–406. https://doi.org/10.3322/CAAC.21693

Mitchell, T., Archer, D. B., Chu, W. T., Coombes, S. A., Lai, S., Wilkes, B. J., McFarland, N. R., Okun, M. S., Black, M. L., Herschel, E., Simuni, T., Comella, C., Xie, T., Li, H., Parrish, T. B., Kurani, A. S., Corcos, D. M., & Vaillancourt, D. E. (2019). Neurite orientation dispersion and density imaging (NODDI) and free-water imaging in Parkinsonism. *Human Brain Mapping*, *40*(17), 5094–5107. https://doi.org/10.1002/HBM.24760

Nazeri, A., Mulsant, B. H., Rajji, T. K., Levesque, M. L., Pipitone, J., Stefanik, L., Shahab, S., Roostaei, T., Wheeler, A. L., Chavez, S., & Voineskos, A. N. (2017). Gray matter neuritic microstructure deficits in schizophrenia and bipolar disorder. *Biological Psychiatry*, *82*(10), 726–736. https://doi.org/10.1016/J.BIOPSYCH.2016.12.005

Niyazi, M., Andratschke, N., Bendszus, M., Chalmers, A. J., Erridge, S. C., Galldiks, N., Lagerwaard, F. J., Navarria, P., Munck af Rosenschöld, P., Ricardi, U., van den Bent, M. J., Weller, M., Belka, C., & Minniti, G. (2023). ESTRO-EANO guideline on target delineation and radiotherapy details for glioblastoma. *Radiotherapy and Oncology*, *184*, 109663. https://doi.org/10.1016/J.RADONC.2023.109663

Okita, Y., Takano, K., Tateishi, S., Hayashi, M., Sakai, M., Kinoshita, M., Kishima, H., & Nakanishi, K. (2023). Neurite orientation dispersion and density imaging and diffusion tensor imaging to facilitate distinction between infiltrating tumors and edemas in glioblastoma. *Magnetic Resonance Imaging*, *100*, 18–25. https://doi.org/10.1016/J.MRI.2023.03.001

Omuro, A., & DeAngelis, L. M. (2013). Glioblastoma and other malignant gliomas: A clinical review. *JAMA*, *310*(17), 1842–1850. https://doi.org/10.1001/JAMA.2013.280319

Onishi, R., Sawaya, R., Tsuji, K., Arihara, N., Ohki, A., Ueda, J., Hata, J., & Saito, S. (2022). Evaluation of temozolomide treatment for glioblastoma using amide proton transfer imaging and diffusion MRI. *Cancers*, *14*(8), 1907. https://doi.org/10.3390/CANCERS14081907

Palacios, E. M., Owen, J. P., Yuh, E. L., Wang, M. B., Vassar, M. J., Ferguson, A. R., Diaz-Arrastia, R., Giacino, J. T., Okonkwo, D. O., Robertson, C. S., Stein, M. B., Temkin, N., Jain, S., McCrea, M., MacDonald, C. L., Levin, H. S., Manley, G. T., & Mukherjee, P. (2020). The evolution of white matter microstructural changes after mild traumatic brain injury: A longitudinal DTI and NODDI study. *Science Advances*, *6*(32), eaaz6892. https://doi.org/10.1126/SCIADV.AAZ6892

Parker, T. D., Slattery, C. F., Zhang, J., Nicholas, J. M., Paterson, R. W., Foulkes, A. J. M., Malone, I. B., Thomas, D. L., Modat, M., Cash, D. M., Crutch, S. J., Alexander, D. C., Ourselin, S., Fox, N. C., Zhang, H., & Schott, J. M. (2018). Cortical microstructure in young onset Alzheimer's disease using neurite orientation dispersion and density imaging. *Human Brain Mapping*, *39*(7), 3005–3017. https://doi.org/10.1002/HBM.24056

Petrecca, K., Guiot, M. C., Panet-Raymond, V., & Souhami, L. (2013). Failure pattern following complete resection plus radiotherapy and temozolomide is at the resection margin in patients with glioblastoma. *Journal of Neuro-Oncology*, *111*(1), 19–23. https://doi.org/10.1007/S11060-012-0983-4

Pollard, S. M., Yoshikawa, K., Clarke, I. D., Danovi, D., Stricker, S., Russell, R., Bayani, J., Head, R., Lee, M., Bernstein, M., Squire, J. A., Smith, A., & Dirks, P. (2009). Glioma stem cell lines expanded in adherent culture have tumor-specific phenotypes and are suitable for chemical and genetic screens. *Cell Stem Cell*, *4*(6), 568–580. https://doi.org/10.1016/J.STEM.2009.03.014

Price, S. J., & Gillard, J. H. (2011). Imaging biomarkers of brain tumour margin and tumour invasion. *The British Journal of Radiology*, *84*(Spec Iss 2), S159. https://doi.org/10.1259/BJR/26838774

Price, S. J., Jena, R., Burnet, N. G., Hutchinson, P. J., Dean, A. F., Peña, A., Pickard, J. D., Carpenter, T. A., & Gillard, J. H. (2006). Improved delineation of glioma margins and regions of infiltration with the use of diffusion tensor imaging: An image-guided biopsy study. *American Journal of Neuroradiology*, *27*(9), 1969–1974. https://doi.org/10.1016/s0513-5117(08)79144-0

Ramesh, K., Mellon, E. A., Gurbani, S. S., Weinberg, B. D., Schreibmann, E., Sheriff, S. A., Goryawala, M., De Le Fuente, M., Eaton, B. R., Zhong, J., Voloschin, A. D., Sengupta, S., Dunbar, E. M., Holdhoff, M., Barker, P. B., Maudsley, A. A., Kleinberg, L. R., Shim, H., & Shu, H. K. G. (2022). A multi-institutional pilot clinical trial of spectroscopic MRI-guided radiation dose escalation for newly diagnosed glioblastoma. *Neuro-Oncology Advances*, *4*(1), vdac006. https://doi.org/10.1093/noajnl/vdac006

Sadeghi, N., D'Haene, N., Decaestecker, C., Levivier, M., Metens, T., Maris, C., Wikler, D., Baleriaux, D., Salmon, I., & Goldman, S. (2008). Apparent diffusion coefficient and cerebral blood volume in brain gliomas: Relation to tumor cell density and tumor microvessel density based on stereotactic biopsies. *American Journal of Neuroradiology*, *29*(3), 476–482. https://doi.org/10.3174/AJNR.A0851

Sanvito, F., Castellano, A., & Falini, A. (2021). Advancements in neuroimaging to unravel biological and molecular features of brain tumors. *Cancers*, *13*(3), 424–424. https://doi.org/10.3390/CANCERS13030424

Schatlo, B., Fandino, J., Smoll, N. R., Wetzel, O., Remonda, L., Marbacher, S., Perrig, W., Landolt, H., & Fathi, A. R. (2015). Outcomes after combined use of intraoperative MRI and 5-aminolevulinic acid in high-grade glioma surgery. *Neuro-Oncology*, *17*(12), 1560–1567. https://doi.org/10.1093/NEUONC/NOV049

Schneider, T., Brownlee, W., Zhang, H., Ciccarelli, O., Miller, D. H., & Wheeler-Kingshott, C. G. (2017). Sensitivity of multi-shell NODDI to multiple sclerosis white matter changes: A pilot study. *Functional Neurology*, *32*(2), 97–101. https://doi.org/10.11138/FNEUR/2017.32.2.097

Seano, G., Nia, H. T., Emblem, K. E., Datta, M., Ren, J., Krishnan, S., Kloepper, J., Pinho, M. C., Ho, W. W., Ghosh, M., Askoxylakis, V., Ferraro, G. B., Riedemann, L., Gerstner, E. R., Batchelor, T. T., Wen, P. Y., Lin, N. U., Grodzinsky, A. J., Fukumura, D., … Jain, R. K. (2019). Solid stress in brain tumours causes neuronal loss and neurological dysfunction and can be reversed by lithium. *Nature Biomedical Engineering*, *3*(3), 230–245. https://doi.org/10.1038/s41551-018-0334-7

Sone, D., Sato, N., Ota, M., Maikusa, N., Kimura, Y., & Matsuda, H. (2018). Abnormal neurite density and orientation dispersion in unilateral temporal lobe epilepsy detected by advanced diffusion imaging. *NeuroImage. Clinical*, *20*, 772–782. https://doi.org/10.1016/J.NICL.2018.09.017

Spano, B., Giulietti, G., Pisani, V., Morreale, M., Tuzzi, E., Nocentini, U., Francia, A., Caltagirone, C., Bozzali, M., & Cercignani, M. (2018). Disruption of neurite morphology parallels MS progression. *Neurology-Neuroimmunology Neuroinflammation*, *5*(6), 502. https://doi.org/10.1212/NXI.0000000000000502

Stepp, H., & Stummer, W. (2018). 5-ALA in the management of malignant glioma. *Lasers in Surgery and Medicine*, *50*(5), 399–419. https://doi.org/10.1002/LSM.22933

Stummer, W., Pichlmeier, U., Meinel, T., Wiestler, O. D., Zanella, F., & Reulen, H. J. (2006). Fluorescence-guided surgery with 5-aminolevulinic acid for resection of malignant glioma: A randomised controlled multicentre phase III trial. *The Lancet Oncology*, *7*(5), 392–401. https://doi.org/10.1016/S1470-2045(06)70665-9

Stupp, R., Mason, W. P., van den Bent, M. J., Weller, M., Fisher, B., Taphoorn, M. J. B., Belanger, K., Brandes, A. A., Marosi, C., Bogdahn, U., Curschmann, J., Janzer, R. C., Ludwin, S. K., Gorlia, T., Allgeier, A., Lacombe, D., Cairncross, J. G., Eisenhauer, E., & Mirimanoff, R. O. (2005). Radiotherapy plus concomitant and adjuvant temozolomide for glioblastoma. *New England Journal of Medicine*, *352*(10), 987–996. https://doi.org/10.1056/NEJMOA043330

Sugahara, T., Korogi, Y., Kochi, M., Ikushima, I., Shigematu, Y., Hirai, T., Okuda, T., Liang, L., Ge, Y., Komohara, Y., Ushio, Y., & Takahashi, M. (1999). Usefulness of diffusion-weighted MRI with echo-planar technique in the evaluation of cellularity in gliomas. *Journal of Magnetic Resonance Imaging*, *9*(1), 53–60. https://doi.org/10.1002/(sici)1522-2586(199901)9:1<53::aid-jmri7>3.0.co;2-2

Thoeny, H. C., & Ross, B. D. (2010). Predicting and monitoring cancer treatment response with diffusion-weighted MRI. *Journal of Magnetic Resonance Imaging*, *32*(1), 2–16. https://doi.org/10.1002/JMRI.22167

Vehlow, A., & Cordes, N. (2013). Invasion as target for therapy of glioblastoma multiforme. *Biochimica et Biophysica Acta (BBA)-Reviews on Cancer*, *1836*(2), 236–244. https://doi.org/10.1016/J.BBCAN.2013.07.001

Venkataramani, V., Tanev, D. I., Strahle, C., Studier-Fischer, A., Fankhauser, L., Kessler, T., Körber, C., Kardorff, M., Ratliff, M., Xie, R., Horstmann, H., Messer, M., Paik, S. P., Knabbe, J., Sahm, F., Kurz, F. T., Acikgöz, A. A., Herrmannsdörfer, F., Agarwal, A., … Kuner, T. (2019). Glutamatergic synaptic input to glioma cells drives brain tumour progression. *Nature*, *573*(7775), 532–538. https://doi.org/10.1038/S41586-019-1564-X

Veraart, J., Fieremans, E., & Novikov, D. S. (2016). Diffusion MRI noise mapping using random matrix theory. *Magnetic Resonance in Medicine*, *76*(5), 1582–1593. https://doi.org/10.1002/MRM.26059

Wang, J., Xu, S. L., Duan, J. J., Yi, L., Guo, Y. F., Shi, Y., Li, L., Yang, Z. Y., Liao, X. M., Cai, J., Zhang, Y. Q., Xiao, H. L., Yin, L., Wu, H., Zhang, J. N., Lv, S. Q., Yang, Q. K., Yang, X. J., Jiang, T., … Yu, S. C. (2018). Invasion of white matter tracts by glioma stem cells is regulated by a NOTCH1–SOX2 positive-feedback loop. *Nature Neuroscience*, *22*(1), 91–105. https://doi.org/10.1038/s41593-018-0285-z

Wang, Z., Zhang, S., Liu, C., Yao, Y., Shi, J., Zhang, J., Qin, Y., & Zhu, W. (2019). A study of neurite orientation dispersion and density imaging in ischemic stroke. *Magnetic Resonance Imaging*, *57*, 28–33. https://doi.org/10.1016/J.MRI.2018.10.018

Wen, Q., Kelley, D. A. C., Banerjee, S., Lupo, J. M., Chang, S. M., Xu, D., Hess, C. P., & Nelson, S. J. (2015). Clinically feasible NODDI characterization of glioma using multiband EPI at 7 T. *NeuroImage: Clinical*, *9*, 291–299. https://doi.org/10.1016/J.NICL.2015.08.017

Winston, G. P., Micallef, C., Symms, M. R., Alexander, D. C., Duncan, J. S., & Zhang, H. (2014). Advanced diffusion imaging sequences could aid assessing patients with focal cortical dysplasia and epilepsy. *Epilepsy Research*, *108*(2), 336–339. https://doi.org/10.1016/J.EPLEPSYRES.2013.11.004

Yi, S. Y., Barnett, B. R., Torres-Velázquez, M., Zhang, Y., Hurley, S. A., Rowley, P. A., Hernando, D., & Yu, J. P. J. (2019). Detecting microglial density with quantitative multi-compartment diffusion MRI. *Frontiers in Neuroscience*, *13*, 81. https://doi.org/10.3389/FNINS.2019.00081

Zhang, H., Schneider, T., Wheeler-Kingshott, C. A., & Alexander, D. C. (2012). NODDI: Practical in vivo neurite orientation dispersion and density imaging of the human brain. *NeuroImage*, *61*(4), 1000–1016. https://doi.org/10.1016/J.NEUROIMAGE.2012.03.072

Zhao, J., Li, J. B., Wang, Y, J., Wang, Y. L., Liu, D. W., Li, X. B., Song, Y. K., Tian, Y. S., Yan, X., Li, Z. H., He, S. F., Huang, X. L., Jiang, L., Yang, Z. Y., & Chu, J. P. (2018). Quantitative analysis of neurite orientation dispersion and density imaging in grading gliomas and detecting IDH-1 gene mutation status. *NeuroImage: Clinical*, *19*, 174. https://doi.org/10.1016/J.NICL.2018.04.011